TONAL FAN NOISE PREDICTION AND VALIDATION ON THE ANCF CONFIGURATION

Marlène SANJOSÉ[1], Majd DAROUKH[2], William MAGNET[2],
Jérôme DE LABORDERIE[2], Stéphane MOREAU[1] and Adrien MANN[3]

[1] *Département de Génie Mécanique, Université de Sherbrooke, 2500 blvd de l'Université, Sherbrooke QC J1K2R1, Canada*

[2] *CERFACS, 42 av. Gaspard Coriolis, 31500 Toulouse, France*

[3] *Aeroacoustics group, Exa Corporation, 150 N Hill Dr., Brisbane CA 94005, USA*

SUMMARY

Three numerical simulations on the NASA Active Noise Control Fan (ANCF) rig have been performed to investigate rotor-stator interaction noise on a realistic turbofan with a high hub-to-tip ratio. These simulations achieved with the PowerFlow solver based on the Lattice Boltzmann Method provide very good direct acoustic prediction for both tonal and broadband noise. The tonal noise directivity is noticeably very well captured. These reliable results are then used to validate the implementation of in-duct rotor-wake interaction noise based on Amiet's analytical isolated blade response, in the in-house OPTIBRUI solver. The required detailed wake excitation is obtained by an averaging procedure that extracts the wake information from the numerical results while removing the potential effect. The analytical results for the rotor-stator interaction compare well with the detailed duct-modes measurements performed on the ANCF configuration. The influence of the stator vane count and the rotor-stator distance of the wake evolution are also emphasized and well captured on these well documented configurations. The precise description of the blade geometry in terms of stagger is also shown to be a key parameter for a realistic noise radiation upstream and downstream.

INTRODUCTION

The NASA Active Noise Control Fan (ANCF) rig has been intensively studied at the Aeroacoustic Propulsion Laboratory facility at NASA Glenn. Measurements have been performed on various stage configurations and flow conditions yielding a large aerodynamic and acoustic database for turbofan noise of high-bypass ratio [1, 2, 3]. Therefore this low hub-to-tip ratio axial fan stage provides an excellent test bed for aeroacoustic code validation of ducted turbomachines with significant modal content. Moreover the relatively low Mach number of the ANCF allows comparing various numerical approaches solving either the Navier-Stokes equations [4] or the Boltzmann equations for the gas

dynamics. Indeed detailed 3D turbulent compressible unsteady simulations have been recently performed on one configuration of this fan stage using a Lattice-Boltzmann Method particularly adapted to low-speed Mach numbers [5, 6]. These simulations including the full geometry of the installation were shown to reproduce the acoustic measurements made in the anechoic facility accurately. They complement the experimental database possibly providing a direct insight into the aerodynamic sources (mainly the rotor wakes impacting on the stator) on top of the in-duct and far-field acoustic propagation.

The present work aims at first extending these initial works to more configurations with various number of stator vanes and rotor-stator distances, and particularly to the 14 stator-vane configuration that provides more detailed flow and acoustic measurements. Some emphasis is put on the possible flow features responsible for the noise generation. Once validated the numerical simulations can then help validating an analytical noise prediction code OPTIBRUI on these well documented ANCF configurations. The software accounts for the complex description of the rotor and stator geometry including varying lean, sweep stagger and camber angles, non-uniformly spaced blades and several analytical models are implemented including free-field or in-duct acoustic propagation models and isolated [7, 8] or cascade blade responses [9] The analytical models require flow modeling as input and the results obtained with analytical, experimental and numerical flow descriptions can then be compared. In particular, the effect of camber is investigated. Some recommendations on the flow extractions from the LBM simulations are also made using the unsteady results.

METHODOLOGY

The rotor wake interactions with the outlet guide vanes is the main tonal contributor to the turbofan noise. The rotor periodic excitation interference with the stator vanes was first shown by Tyler & Sofrin [10]. This noise mechanism can be captured with analytical acoustic models: a blade response to the distortion harmonics of the rotor wakes is propagated into the duct of the turbofan to provide the upstream and downstream acoustic levels. The precise description of the rotor excitation interacting on the stator leading-edge is the key parameter to capture the stator lift fluctuations accurately.

The wakes can be modeled using Gaussian models whose shape and evolutions are based on empirical or semi-empirical models [11, 12, 13]. The high swirl flow in the rotor-stator space and the tip and hub secondary flows make the prediction of the rotor wake that interacts with the stator vanes very challenging to predict in a practical case [12, 14].

In the present work, the excitation is extracted from the LBM numerical simulations performed on the ANCF configuration. The evolution of the wakes in the inter-stage realistic flow, the effect of the secondary flows and of the potential effects from the stator row will be analyzed in the result section. The details of the simulations and of the analytical model used for the acoustic predictions are presented in the next two paragraphs.

Numerical simulations

The present simulations use the PowerFlow solver 5.0a based on the Lattice Boltzmann Method (LBM). The approach is naturally transient and compressible providing a direct insight into hydrodynamics mechanisms responsible for the acoustic sources but also into acoustic propagation in the nacelle and outside in the free-field.

Instead of studying macroscopic fluid quantities, the LBM tracks the time and space evolution on a lattice grid of a truncated particle distribution function. The particle distribution evolution is driven

to the equilibrium by the so-called collision operator, approximated by the BGK model. The discrete Lattice-Boltzmann equations needs to be solved for a finite number of particle velocity. The discretization retained in Powerflow involves 19 discrete velocities for the third order truncation of the particle distribution function, which has been shown sufficient to recover the Navier-Stokes equations for a perfect gas at low Mach number in isothermal conditions[15, 16, 17]. In Powerflow, a single relaxation time is used, which is related to the dimensionless laminar kinematic viscosity [18]. This relaxation time is replaced by an effective turbulent relaxation time that is derived from a systematic Renormalization Group procedure detailed in [19]. It captures the large structures in the anechoic room but also the small turbulent scales that develop along the blade and duct surfaces where law of the wall boundary conditions accounting for pressure gradients are applied using specular reflections [20]. The particular extension of the method developed for rotating machines can be found in Zhang *et al.* [21].

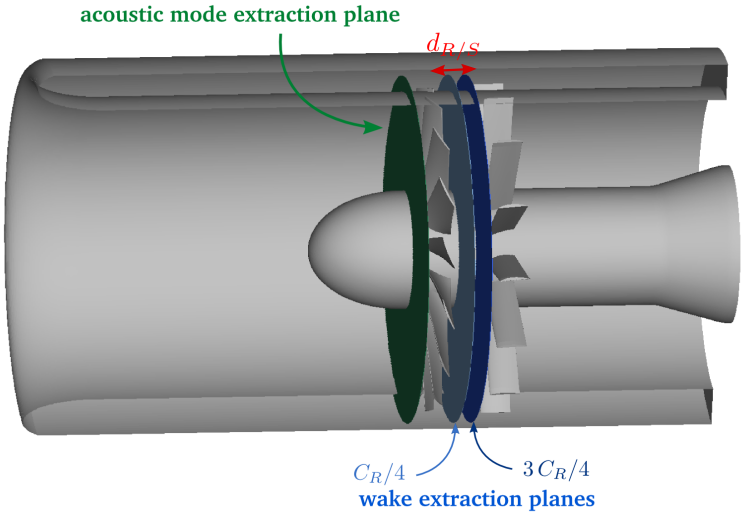

Figure 1: Simulated geometry and extraction planes.

With this method, the flow field is computed on the full test-rig of the Aero-Acoustic Propulsion Laboratory at NASA Glenn [1, 2, 3]. Only the rotor driving system and the measurement system are not considered in the setup as shown in Fig. 1 The actual laboratory is also replaced by a very large, 132x113x113 m wide, anechoic room. The present full setup is based on the initial model provided by EXA and used in previous studies [5, 6]. The configuration includes the 1.22 m diameter duct with the precise geometry for the bellmouth and the hub. The study focuses on the nominal fan conditions: the fan has $B = 16$ blades with a 28° pitch angle at the hub, and is rotating at $\Omega = 1800$ rpm. The tip clearance of 0.05% fan diameter is ignored by extruding the blades to the duct. The finest grid resolution around the rotor and stator is 0.1% fan diameter and 0.2% fan diameter in the inter-stage space. In the original setup [6, 5] the rotor-stator distance measured at the hub was $0.3\,C_R$ and the stator vane count was 13. In the present simulations, several stator configurations have been investigated to compare with the ANCF experimental database, summarized in Tab. 1. The rotor-stator distance $d_{R/S}$ is measured at the hub and given in terms of rotor chord C_R. The simulation timestep is 2.44×10^{-6} s. A transient time of 10 fan rotations is observed. Volume measurements are recorded in the rotor-stator vicinity 26 times per blade passing period $T_{bpp} = 1/B\Omega$. Velocity components of the wake flow are recorded at higher-rate every $T_{bpp}/213$ on a disk located at $C_R/4$ downstream from the rotor trailing-edge as shown in Fig. 1. In the case of the 14-C simulation, an additional plane is located at $3\,C_R/4$.

Simulation Id	Vane count	Rotor-Stator distance
13-HC	13	$d_{R/S} = C_R/2$
14-HC	14	$d_{R/S} = C_R/2$
14-C	14	$d_{R/S} = C_R$

Table 1: Summary of performed simulations.

Analytical model

This section presents the tonal analytical model used for the acoustic prediction and comparison with experimental measurements and numerical results. This model is integrated in the OPTIBRUI software for noise prediction of axial turbomachine developed at Université de Sherbrooke.

The stator is mounted in an infinite annular duct of constant section. The cylindrical reference frame $\mathcal{R}_d(r_d, \theta_d, z_d)$ is fixed to the duct with its axial direction corresponding to the machine axis oriented towards the exhaust of the duct. In order to account for the complex blade geometry, the vane is split into several annular strips of identical span dr. At each strip r_d, the blade element is described as a flat plate of constant chord $C\,(r_d)$ and stagger angle $\chi\,(r_d)$. The radial stacking of the blade elements is parameterized by the lean and sweep angles ($\varphi_{LE}(r_d)$,$\psi_{LE}(r_d)$) that define the location of the blade element leading-edge with respect to a rotational and a meridional plane crossing the blade leading-edge at the hub. Each annular strip can be unwrapped into a rectilinear cascade geometry. A local Cartesian reference frame $\mathcal{R}_c(x_c, y_c, z_c)$ is defined to compute the blade element acoustic response.

For the acoustic propagation, the rotational speed of the machine being low, the swirl effects are ignored. Only an inviscid mean axial flow of Mach number M_a is considered. Within these assumptions, Goldstein's analogy [8] provides the acoustic pressure in the duct resulting from the force $\vec{f}$ exerted by the blade surface S on the fluid using the annular duct Green's function G:

$$p(\vec{x}, t) = \int_{-T}^{T} \iint_{S} \frac{\partial G\,(\vec{x}, t|\vec{x_0}, t_0)}{\partial x_{0,i}}\, f_i\,(\vec{x_0}, t_0)\, dS\,(\vec{x}_0) dt_0 \tag{1}$$

with T a large but finite time period sufficient to capture all the aerodynamic effects on the sound, t_0 and t the emission and observer times and $\vec{x}_0$ and $\vec{x}$ the emission and observer positions respectively in the duct coordinate system.

The Green's function can be written on the duct mode basis using the indices n and j for the circumferential and radial modes respectively in the frequency space:

$$G\,(\vec{x}, t|\vec{x_0}, t_0) = \frac{\mathbf{i}}{4\pi} \sum_{n=-\infty}^{+\infty} \sum_{j=0}^{+\infty} \frac{E_{nj}(r_0)\, E_{nj}(r)\, e^{\mathbf{i}n(\theta-\theta_0)}}{\Gamma_{nj}} \int_{-\infty}^{\infty} \frac{e^{-\mathbf{i}\left(\gamma_{nj}^{\pm}(x-x_0)+\omega(t-t_0)\right)}}{\kappa_{nj}} d\omega \tag{2}$$

with $k_0 = \omega/c_0$, E_{nj} the duct radial function depending on the eigenvalue χ_{nj} of norm $\Gamma_{nj}/2\pi$, $\gamma_{nj}^{\pm} = \frac{M_a k_0 \pm \kappa_{nj}}{\beta^2}$ the axial acoustic wavenumber and $\kappa_{nj}^2 = k_0^2 - \beta^2\chi_{nj}^2$ the cut-off criteria. The superscript $\pm$ is related to the direction of propagation for $z > z_0$ and $z < z_0$ respectively.

The force can be related to the pressure jump across the blade: $\vec{f} = \Delta P \vec{n}$ with $\vec{n} = -\text{sign}\,(\Omega)\,\vec{e}_{y,c}$ the local normal of the blade pointing towards the suction side. Because of the low count of stator, an isolated blade response model is used to compute the pressure jump. In the present work only gusts parallel to the stator are considered, and the deterministic gusts are periodic. Thus it can be decomposed into a Fourier series to account for the wake passing periodicity. The Fourier coefficient for the positive harmonic frequency $mB\,|\Omega|$ is computed at each strip along the flat plate and is written $\widehat{\Delta P}_{mB}\,(r_d, z_d)$.

As the acoustic source are fixed in the duct reference frame, the order of integrals in Eq. (1) can be exchanged. Then for a rotation period integration and uniformly distributed rotor blades the acoustic pressure becomes the summation of tones at the blade passing frequency. The acoustic pressure at the positive harmonic frequency $mB\,|\Omega|$ writes:

$$\widehat{p^{\pm}}\left(r_d,\theta_d,z_d,t\right)=\sum_{n=-\infty}^{+\infty}\sum_{j=0}^{+\infty}E_{nj}(r)\,e^{\mathbf{i}\left(n\theta_d-\gamma_{nj}^{\pm}z_d\right)}P_{nj,mB}^{\pm}\,e^{-\mathbf{i}mB|\Omega|t} \tag{3}$$

Assuming that the V stator vanes are uniformlly distributed, the double infinite sum in Eq.(3) is limited to the acoustic duct modes (n,j) excited by the rotor-stator interaction following Tyler & Sofrin [10, 9] relation adapted for any rotation sign:

$$\text{sign}(\Omega)mB-n=zV \qquad \text{with: } z\in\mathbb{Z} \tag{4}$$

The modal coefficient $P_{nj,mB}^{\pm}$ can be computed by splitting the summation first along the circonferential extent of the blade then along its span.

$$\begin{aligned}P_{nj,mB}^{\pm} &= \frac{\text{sign}(\Omega)V}{2\Gamma_{nj}\kappa_{nj}}\int_{R_H}^{R_T}\left\{-\mathbf{i}Q_{23}\frac{\partial}{\partial r_0}-\frac{n}{r_0}Q_{22}+\gamma_{nj}^{\pm}Q_{21}\right\}E_{nj}(r_0)\\ &\times\; e^{\mathbf{i}\left(\gamma_{nj}^{\pm}z_{d,LE}(r_0)-n\theta_{d,LE}(r_0)\right)}I_{nj,mB}^{\pm}dr_0\end{aligned} \tag{5}$$

with Q the transformation matrix from the $\mathcal{R}_d$ to $\mathcal{R}_c$ reference frames. The chordwise integral $I_{nj}^{\pm}$ is approximated assuming a chordwise wavenumber without sweep nor lean effects. Following the acoustic flat plate response of Amiet & Patterson [22], the pressure jump chordwise integral can be computed analytically and related to the harmonics of the incident upwash velocity gust w_{mB} seen by the leading-edge of the blade.

$$I_{nj,mB}^{\pm}=\frac{C}{2r_0}\int_0^2\widehat{\Delta P}_{mB}(x_c^*)e^{\mathbf{i}\frac{C}{2}\left(\frac{n}{r_0}\sin\chi_S+\gamma_{nj}^{\pm}\cos\chi_S\right)x_c^*}dx_c^*=2\pi U\,\widehat{w}_{mB}\left(\mathcal{L}_{nj}^1+\mathcal{L}_{nj}^2\right) \tag{6}$$

where U is the absolute velocity and $\mathcal{L}_{nj}^1$ and $\mathcal{L}_{nj}^2$ are the blade response and back-scattering from the trailing-edge respectively for supercritic gusts defined in [23].

Finally the acoustic power at the harmonic m reads after integration on a duct section [24]:

$$\Pi_{mB}^{\pm}=\sum_{n=-\infty}^{+\infty}\sum_{j=0}^{+\infty}\frac{\Gamma_{nj}\beta^4k_0\kappa_{nj}}{\rho_0c_0\left(k_0\pm M_a\kappa_{nj}\right)^2}\left|P_{nj,mB}^{\pm}\right|^2 \tag{7}$$

RESULTS

Flow topology

In the three performed calculations, the flow topology of the rotor-stator interaction has the same features. An unrolled blade-to-blade surface at midspan of an instantaneous field of the simulations is shown in Fig. 2. The trace of the rotor wakes is strong and persist to the stator leading-edge where it is chopped[1]. The wakes interact with the stator-vane circulation inducing lift fluctuations. The

[1]It must stressed that the field discontinuity at the rotor-stator interface is only a post-processing effect as projected nodal values were manipulated while the simulation data are computed at the element center.

wakes impact with slightly lower velocity deficits. The pressure fields shown in the bottom pictures of the unrolled maps show how strongly the potential field from the stator influences the rotor. The strongest interaction seems to appear for the 13-HC simulation where strong distortions from passage to passage can be identified. The 14-C simulation shows the least distorted pressure field.

The secondary flows can be identified using the Q-criterion computed in the local reference frames of each blade row, where Q stands for the second invariant of the velocity-gradient tensor. Similar structures have been identified in the three simulations, and only the visualization made for the 14-C simulation is shown in Fig. 3 as the larger inter-stage spacing allows for a clearer identification. First on the rotor, two tip-vortex structures can be identified. Close to the leading-edge the tip leakage vortex is very limited (similar to a distorted horse-shoe vortex) as the tip-gap geometry has been closed artificially. The tip separation vortex is thin but very coherent and interacts with the stator tip leading-edge. On the hub a corner vortex can be observed. It is quite coherent and propagates towards the stator hub leading-edge. On the stator, the wake interaction can be clearly identified by the swept trace on the suction side. The blade rotor has a varying stagger from hub to tip inducing a longer convection time for the wake part impacting at the tip than the one impacting at the hub. Two major flow separations (cornex vortices) can also be observed at the tip and foot of the stator. Similar flow patterns have been observed and investigated in detail in Pasco *et al.* [4] and Guedeney & Moreau [25].

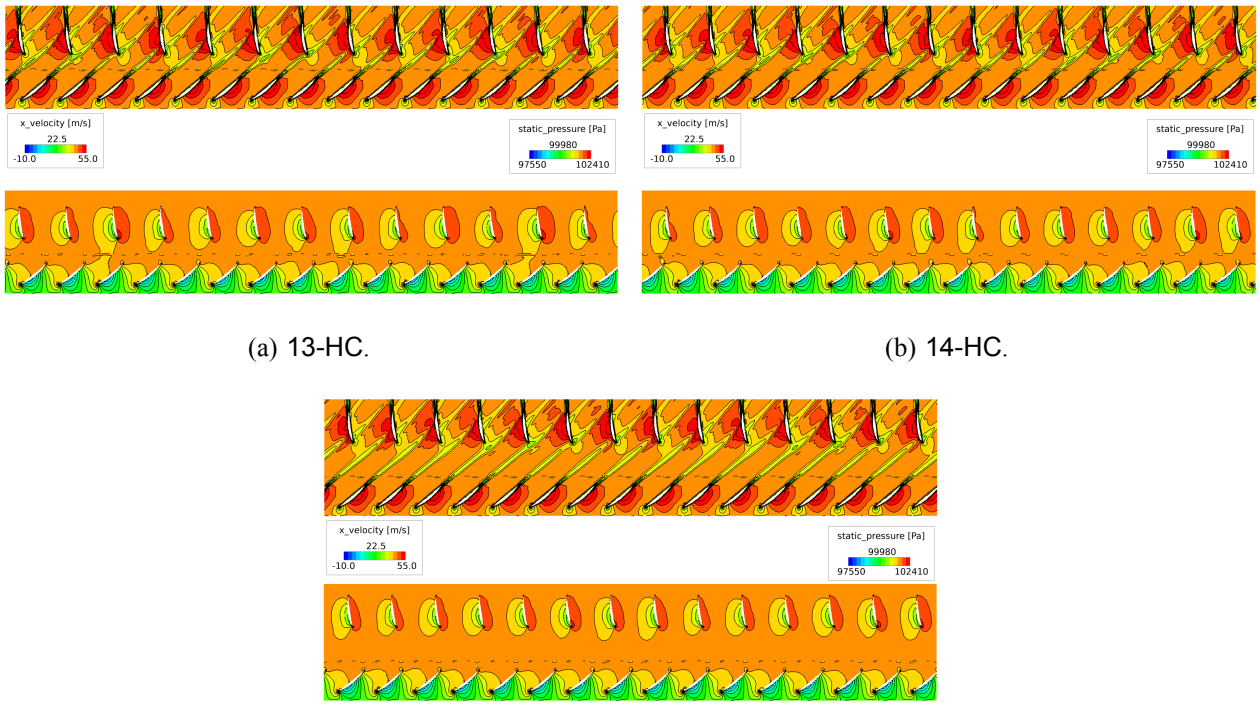

(a) 13-HC.

(b) 14-HC.

(c) 14-C.

Figure 2: Instantaneous flow visualization on an unrolled blade-to-blade surface at mi-span of the duct. Top: contours of the axial component of the absolute velocity. Bottom: static pressure contours.

Wake evolution and potential effects

The main input of the analytical model is the harmonics excitation coming from the wake. As already observed in Fig. 2 the potential effect coming from the stator vanes is quite strong and might influence the excitation. The wakes have been extracted at different spanwise positions from the rotor trailing edge to the stator leading-edge from an instantaneous field in the three simulations. The Fourier

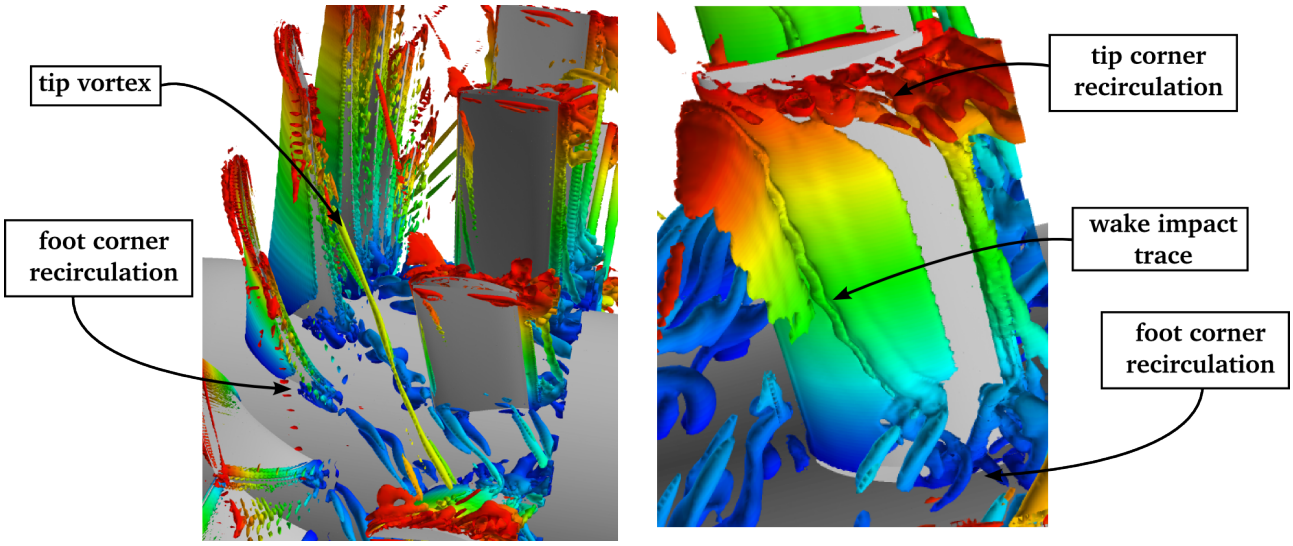

*Figure 3: Snapshot of the flow structures identified by an iso-surface of Q-criterion computed in the local reference frames $Q = 2\times10^6 s^-1$ colored by the radius for the **14-C** simulation. Left: rotor-stator visualisation observed from downstream, right: suction side of the stator.*

coefficients of the periodic signals have been computed. The evolution of the first and secondary rotor blade harmonics are shown in Fig. 4 for the three simulations.

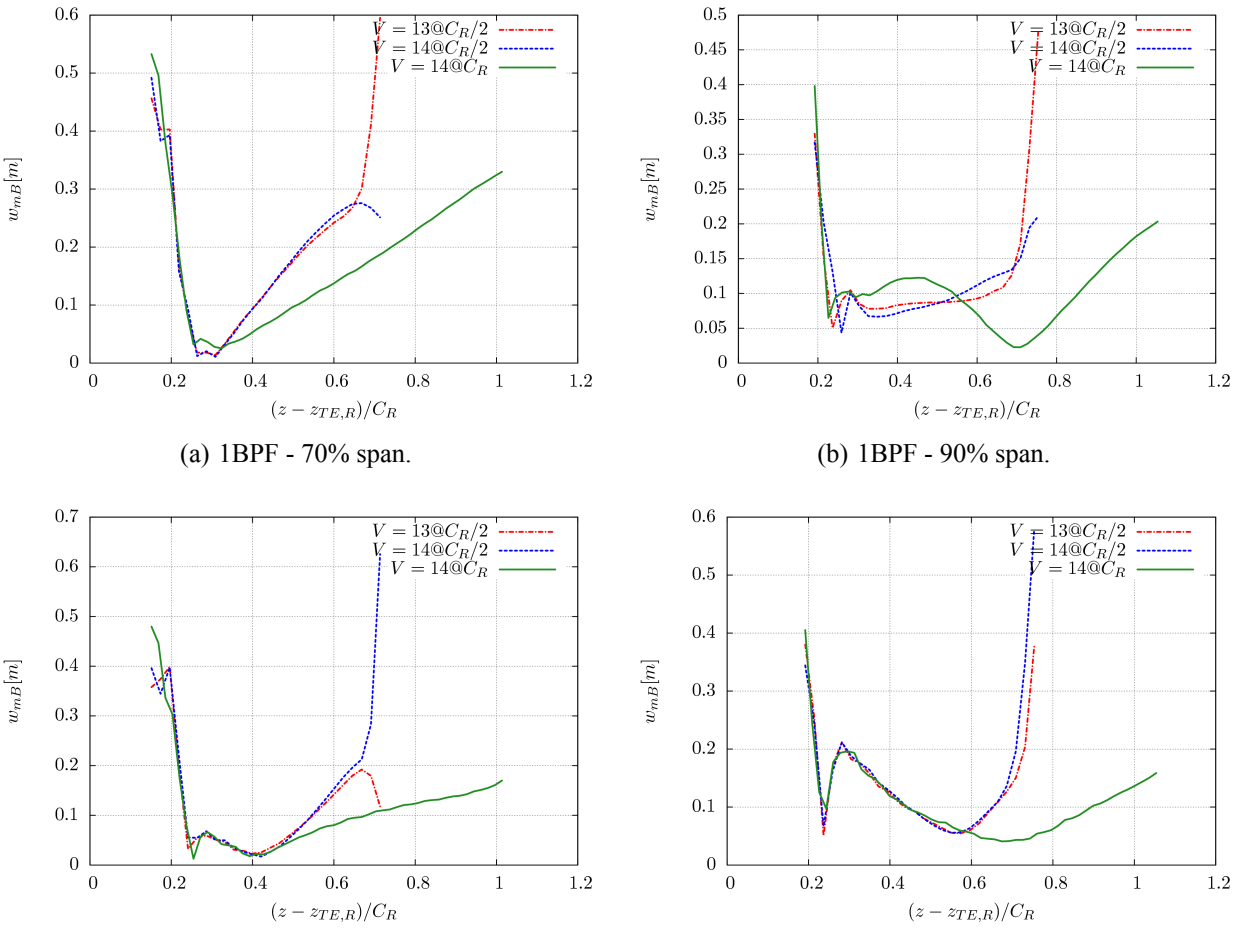

(a) 1BPF - 70% span.

(b) 1BPF - 90% span.

(c) 2BPF - 70% span.

(d) 2BPF - 90% span.

Figure 4: Evolution of the rotor wake Fourier coefficients along the machine axis.

The wake coefficients of the first rotor blade harmonics are the most affected by the potential effects. The differences between the 13-HC and 14-HC case are very limited to the stator vicinity, while the differences with the 14-C setup appear starting from a distance $C_R/3$ of the rotor trailing-edge. The wake Fourier coefficient can be between 20% to 70% different.

This is thus very important to remove this effect to prescribe the proper rotor wake excitation in the acoustic model. The wakes are extracted in a vertical plane at integer numbers of rotation. The rotor wakes are time averaged in the rotor reference frame. The stator sweeps a full rotation thus its potential effect is averaged and does not contribute in the distortion harmonics anymore. The upwash absolute velocity at the blade leading edge is computed using the precise definition of the stator at each blade strip. The coefficients of the upwash velocity for the three calculations (including the one computed on the furthest plane for the 14-C calculation) are given in Fig. 5. The 14-HC and 14-C computed at the same distance from the rotor agree very well showing that the averaging procedure is well adapted to remove the potential effect. The excitation computed in the downstream plane for the 14-C calculation show lower levels, showing that the upwash fluctuations decrease while convecting towards the stator. Surprisingly, the amplitudes for the 13-HC case are very low while recorded at the same location as the 14-HC case.

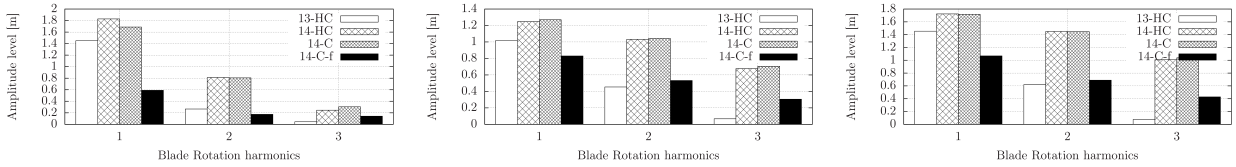

(a) 5% span. (b) 50% span. (c) 95% span.

Figure 5: Wake Fourier coefficients used in the analytical calculations.

Acoustic results

The far-field results directly measured in the calculations with probes located at 3 rotor diameter from the rotor axis are first compared to the far-field acoustic measurements performed at the same locations. The experimental data is acquired on 20 s with a sampling frequency of about 7680 Hz (256 times per revolution). The numerical data is acquired with a sampling frequency of about 5,000 Hz on 0.5 s. The numerical spectra using the Welch's algorithm with 8 overlapping windows yields a spectra with 6.5 Hz of resolution. For the experimental data, the chunk size in the Welch's algorithm is adapted to results in a similar spectral resolution. In the ANCF database recorded in 2008, the 13-HC configuration has not been kept, but had been intensively investigated in 1996 by Sutliff *et al.* [1].

The direct acoustic predictions show once again that the LBM solver is well adapted for the aeroacoustics of low-speed rotating machines. The low dissipation of the method allows capturing the first three blade passing frequencies in the spectra within 5 to 8 dB accuracy. The simulation 14-C yields lower levels for the first BPF than the 14-HC in agreement with the experimental observations. The direct LBM noise prediction is therefore able to reproduce the experimental trends. The broadband noise levels are under-predicted with 10 dB accuracy up to 1000 Hz (maximum resolved frequency for a voxel size of 12 mm and 12 points per wavelength [5]). It could be related to the inaccurate representation in the simulation of the tip gap or other small details in the mockup geometry. Also a higher resolution would certainly helps to better resolve the turbulence levels in the wake, redistributing some energy from the tones to the broadband noise level. In particular the broadband level of the experiments is slightly better captured in the 14-HC simulation than in the 14-C stressing the effect

of a slightly over-predicted dissipation of the rotor turbulent wakes.

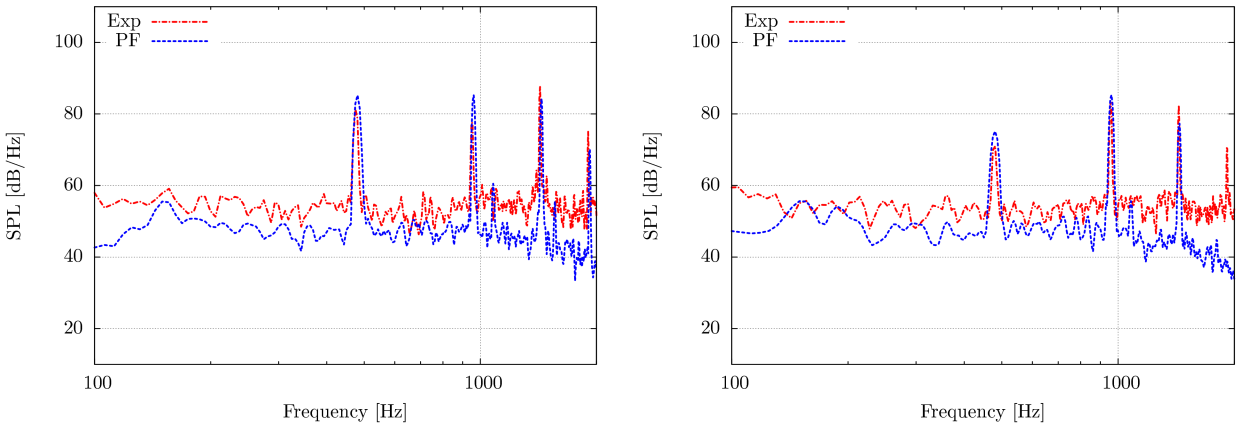

(a) 14-HC. (b) 14-C.

Figure 6: Acoustic spectra measured at 4 m from the rotor axis, at 125° downstream from the rotor axis.

The directivity of the first and second harmonics is given in Fig. 7. Both tone directivities are correctly captured, within 5dB of the main lobes. In particular the lower levels downstream for the 14-C setup demonstrate that the in-duct acoustic propagation is well reproduced by the simulations. Some additional sources might be missing to reproduce the directivity in the range 60°-120° and could also be related to installation effects in the experiments.

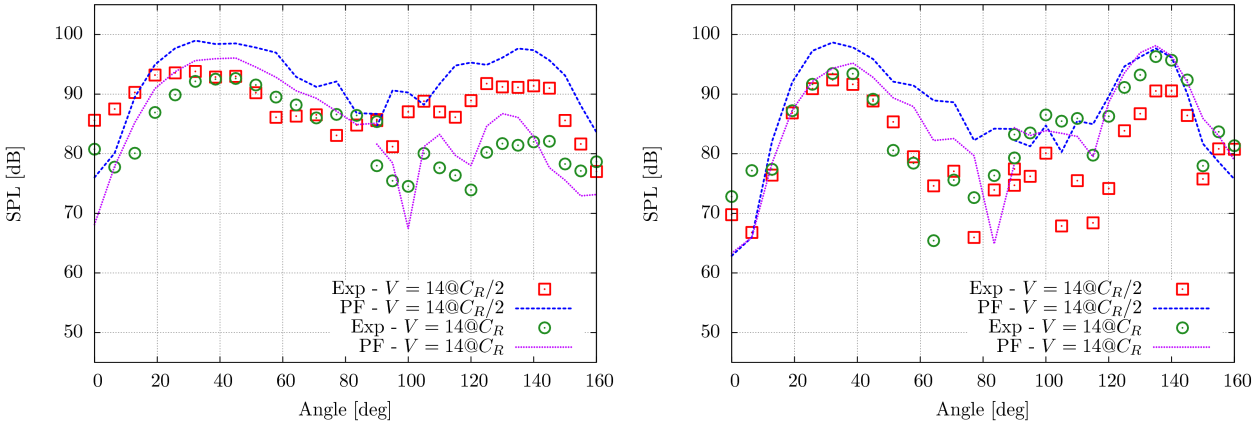

(a) 1 BPF. (b) 2 BPF.

Figure 7: Directivity of the tonal noise measured at 4 m from the rotor axis, upstream and downstream of the fan.

In a plane upstream of the rotor located in the annular section shown in Fig. 1, the pressure is recorded on a rake of 50 points in radius and 180 points in azimuth over three fan rotation periods. Time and azimuthal Fourier transforms are performed to obtain the azimuthal pressure coefficients $p_{n,s}$ evolution over the radius for each harmonics mB. This coefficient is projected onto the infinite annular duct-modes $E_{n,j}$ basis using the Moore-Penrose pseudo-inversion to obtain the pressure modal amplitude P_{nj}. Applying the scaling shown in the sums of Eq. 7, the power modal amplitude upstream and downstream can be extracted from the simulations.

The acoustic propagation inside the duct has been investigated in the ANCF configuration [2, 26, 27]. This database is used to compare with the power modal amplitude extracted from the simulations and

predicted with the analytical model based on the wake distortion and the incoming absolute velocity extracted from the simulations. For each case, the OPTIBRUI analytical tool has been applied on the stator vanes discretized into 19 strips. In the case of the 14-C configuration, the two extractions are compared. Each strip, considered as an infinite flat plate, has its own stagger angle. Lean and sweep are also considered but very small in the present geometry. For each case, two stagger angle values are considered: the stagger angle χ of the flat plate from the leading-edge to the trailing-edge, and a modified value accounting for the camber of the profile. In the latter case $\chi' = \chi + 0.9\sigma_{LE} + 0.1\sigma_{TE}$ to better fit the leading-edge orientation where most of the diffraction occurs. The results are compared for the acoustic modes propagating upstream with experimental results in Figs. 8, 9 and 10. With the analytical model, the acoustic modal power is over-predicted up to 10 depending on the configuration. The predictions computed from the wake extraction closer to the leading-edge of the stator provide the best agreement for the 14-C configuration, highlighting that the wake evolution has a strong effect. The modification of the stagger angle by the camber at the leading-edge is globally providing a better agreement, radiating less energy upstream, which is consistent with the findings of de Laborderie *et al.* [28]. Still on some modes, the effect is not clear or may degrade the agreement. The mode extracted from the numerical simulations show a good agreement within 5 to 10 dB to the experiment mode amplitudes. In the analytical prediction the acoustic propagation is computed for an infinite duct missing the damping effects from the inlet of the nacelle.

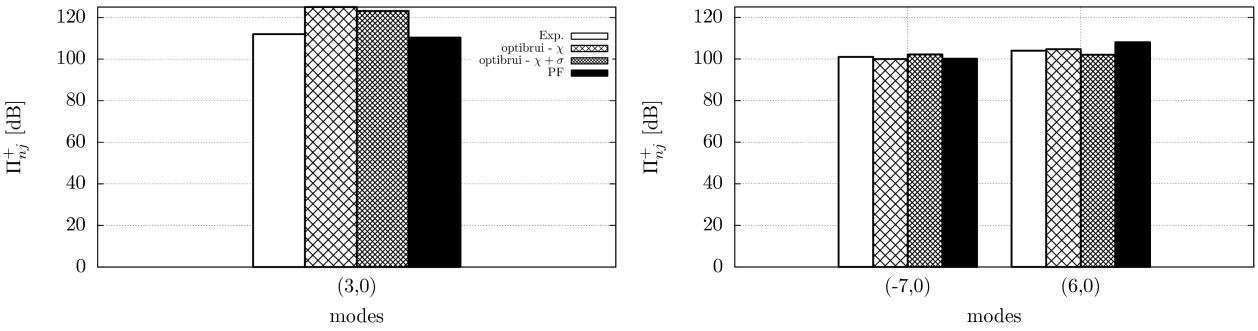

(a) 1 BPF (b) 2 BPF

Figure 8: Acoustic modes predicted upstream in the 13-HC configuration.

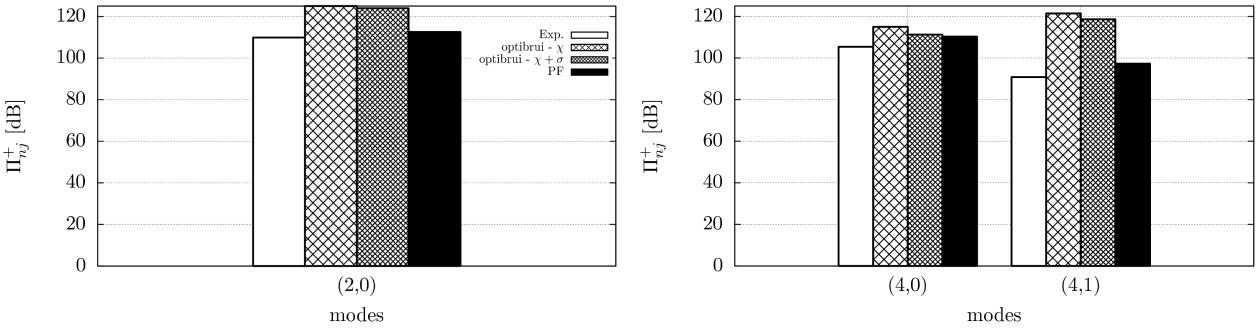

(a) 1 BPF (b) 2 BPF

Figure 9: Acoustic modes predicted upstream in the 14-HC configuration.

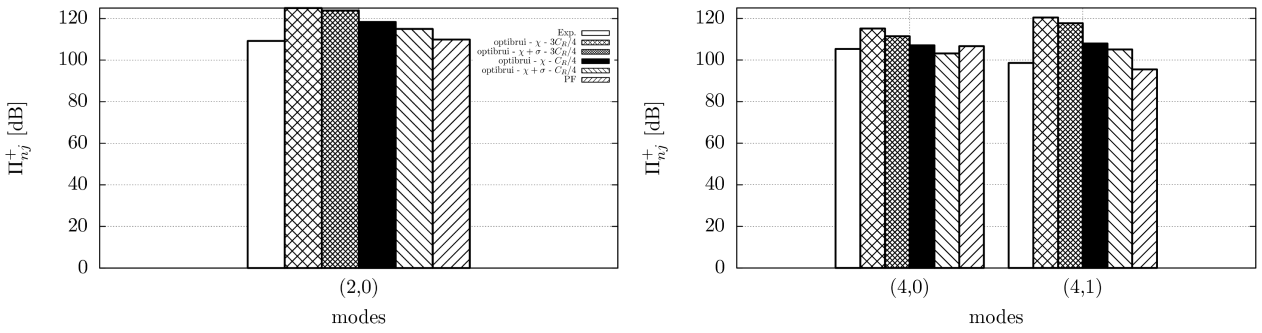

(a) 1 BPF (b) 2 BPF

Figure 10: Acoustic modes predicted upstream in the 14-C configuration.

CONCLUSIONS

In the present work three numerical LBM simulations on the NASA-ANCF configurations have been performed to investigate the rotor-stator interaction in a realistic turbofan, which complements some prior works on a single configuration [6, 5]. The selected ANCF test-bed provides a large and open experimental database for the validation of aeroacoustic tools. The configuration is also very representative of turbofan with a high hub-to-tip ratio. Only the rotational speed and the operating Mach number are low, which makes it an excellent test-bed for several numerical methods. The direct LBM noise predictions with PowerFlow are in very good agreement with the available experimental data for all 3 configurations providing confidence in the numerical simulations that are then used to validate the OPTIBRUI aeroacoustic tool developed by Université de Sherbrooke. The latter uses the wake distortion inputs from the numerical simulations of the three configurations that have different stator vane counts and rotor-stator spacings. The rotor-stator interaction in the simulations is first analyzed and the emphasis is put on the potential effects from the stator vanes. This effect biases the extraction of the rotor wakes from the CFD results. To overcome the potential effect, an averaging procedure in the rotor frame of reference has been implemented. The far-field acoustic results directly predicted in the simulations are compared with the experimental database. The simulations capture both the tonal and broadband noise very well. Even the directivity of the tones is well predicted and the trend between the different configuration is well reproduced. The simulations accurately resolve the rotor-stator interaction, and the acoustic propagation first in the duct, then in free-field. The velocity fields extracted from these simulations are therefore reliable inputs for the acoustic validation of OPTIBRUI. A strip theory with Amiet's analytical response [7] for isolated flat plates is used to discretize the stator blade geometry, and the acoustic power upstream and downstream of the fan is obtained by using Goldstein's acoustic analogy [8]. The resulting in-duct acoustic powers compare well with the measurements, particularly for the second harmonics that is predicted within 5 dB. The correction on the stagger angle accounting for the camber also improves the predictions. Therefore reliable rotor-stator interaction noise predictions can be performed with OPTIBRUI at the design stage.

ACKNOWLEDGEMENTS

Computations were made on the supercomputer Mammouth-MP2 from Université de Sherbrooke, managed by Calcul Québec and Compute Canada. The operation of this supercomputer is funded by the CFI, NanoQuébec, RMGA and FRQ-NT. The authors would like to thank D. Sutliff from NASA for providing us with the ANCF geometry and experimental data, and F. Pérot from Exa for fruitful

discussions and technical support. Finally they would like to acknowledge Airbus, Safran and Valeo partners of the aeroacoustic industrial Chair of the Université de Sherbrooke funding this research project.

REFERENCES

[1] D. L. Sutliff, L. J. Heidelberg, D. M. Elliott, and M. Nallasamy. *Baseline acoustic levels of the* NASA *active noise control fan rig*. In *Second AIAA/CEAS Aeroacoustics Conference*, number AIAA-1996-1745, NASA-TM-107214, **1996**.

[2] L. J. Heidelberg, D. G. Hall, J. E. Bridges, and M. Nallasamy. *A unique ducted fan test bed for active noise control and aeroacoustic research*. In *Second AIAA/CEAS Aeroacoustics Conference*, number AIAA-1996-1740, NASA-TM-107213, **1996**.

[3] J. McAllister, R. A. Loew, J. T. Lauer, and D. L. Sutliff. *The advanced noise control fan baseline measurements*. In *47th Aerospace Science Meeting*, number NASA-TM-215595, AIAA-2009-0624, **2009**.

[4] Y. Pasco, T. Guedeney, A. Leung-Tak, A. Berry, S. Moreau, and P. Masson. *Active noise control simulation of tonal turbofan noise in aero engines*. In *20th AIAA/CEAS Aeroacoustics Conference*, number AIAA-2014-3187, Atlanta, GA, **2014**.

[5] A. Mann, F. Pérot, M-S. Kim, D. Casalino, and E. Fares. *Advanced Noise Control Fan Direct Aeroacoustics Predictions Using a Lattice-Boltzmann MethodM-S. KimD. CasaliE. Fare*. In *18th AIAA/CEAS Aeroacoustics Conference*, AIAA-2012-2287, Colorados Springs, CO, June **2012**.

[6] A. L. P. Maldonado, R. F. Bobenrieth Miserda, and B. G. Pimenta. *Computational Tonal Noise Prediction for the Advanced Noise Control Fan*. In *18th AIAA/CEAS Aeroacoustics Conference*, AIAA 2012-2128, Colorado Springs, CO, June **2012**.

[7] R. K. Amiet. *High frequency thin-airfoil theory for subsonic flow*. AIAA J., 14(8):1076--1082, **1976**.

[8] M. E. Goldstein. *Aeroacoustics*. McGraw-Hill, Inc, **1976**.

[9] J. de Laborderie. *Approches analytiques et numériques pour la prédiction du bruit tonal et large bande de soufflantes de turboréacteurs*. PhD thesis, Université de Sherbrooke, Sherbrooke, QC, CANADA, September **2013**.

[10] J. M. Tyler and T. G. Sofrin. *Axial flow compressor noise studies*. Society of Automotive Engineers Transactions, 70:309--332, **1962**.

[11] R. Raj and B. Lakshminarayana. *Three Dimensional Characteristics of Turbulent Wakes Behind Turbomachinery Rotors*. J. Eng. Power, 98(2):218--228, **1976**.

[12] R. K. Majjigi and P. R. Gliebe. *Development of a rotor wake/vortex model*. Technical Report 174849, NASA, Lewis Research Center, Ohio, USA, June **1984**.

[13] D. A. Philbrick and D. A. Topol. *Development of a Fan Noise Design System Part 1: system design and source modeling*. In *15th AIAA Aeroacoustics Conference*, AIAA-93-4415, Long Beach, CA, October **1993**.

[14] J. Cooper and N. Peake. *Upstream-radiated rotor--stator interaction noise in mean swirling flow*. J. Fluid Mech., 523:219--250, **2005**.

[15] U. Frisch, D. D'Humiéres, B. Hasslacher, P. Lallemend, Y. Pomeau, and J-P. Rivet. *Lattice gas hydrodynamics in two and three dimensions*. Complex Syst., 1:649--707, **1987**.

[16] S. Chen and G. D. Dooler. *Lattice Boltzmann method for fluid flows*. Ann. Rev. Fluid Mech., 30:329--364, **1998**.

[17] S. Marié, D. Ricot, and P. Sagaut. *Comparison between lattice Boltzmann method and Navier-Stokes high order schemes for computational aeroacoustics*. J. Comp. Phys., 228:1056--1070, **2009**.

[18] E. Vergnault, O. Malaspinas, and P. Sagaut. *A lattice Boltzmann method for nonlinear disturbances around an arbitrary base flow*. J. Comput. Phys., 231:8070--8082, **2012**.

[19] H. Chen, S. A. Orszag, I. Staroselsky, and S. Succi. *Expanded analogy between Boltzmann kinetic theory of fluids and turbulence*. J. Fluid Mech., 519:301--314, November **2004**.

[20] H. Chen, C. Teixeira, and K. Molvig. *Realization of Fluid Boundary Conditions via Discrete Boltzmann Dynamics*. International Journal of Modern Physics C, 09(08):1281--1292, **1998**.

[21] R. Zhang, C. Sun, Y. Li, R. Satti, R. Shock, J. Hoch, and H. Chen. *Lattice Boltzmann Approach for Local Reference Frames*. Commun. Comput. Phys., 9(5):1193--1205, **2011**.

[22] R. W. Paterson and R. K. Amiet. *Acoustic radiation and surface pressure characteristics of an airfoil due to incident turbulence*. Technical Report NASA-CR-2733, NASA, **1976**.

[23] G. Reboul. *Modélisation du bruit à large bande de soufflante de turboréacteur*. PhD thesis, Ecole Centrale de Lyon, **2010**.

[24] H. D. Meyer and E. Envia. *Aeroacoustic analysis of turbofan noise generation*. Technical Report NASA-CR-4715, NASA, **1996**.

[25] T. Guedeney and S. Moreau. *Unsteady RANS simulations of a low speed fan for analytical tonal noise prediction*. In *11th European Turbomachinery Conference*. Madrid, Spain, **2015**.

[26] L. J. Heidelberg. *Fan noise source diagnostic test - tone modal structure results*. In *8th AIAA/CEAS Aeroacoustics Conference*, volume AIAA-2002-2428, Breckenridge, CO, **2002**.

[27] D. L. Sutliff. *Rotating rake turbofan duct mode measurement system*. Technical Report NASA-TM-2005-213828, NASA, **2005**.

[28] J. de Laborderie, V. Blandeau, T. Node-Langlois, and S. Moreau. *Extension of a Fan Tonal Noise Cascade Model for Camber Effects*. AIAA J., posted online, **2015**.